

Triplet Upconversion Under Ambient Conditions Enables Digital Light Processing 3D Printing

Connor J. O’Dea, Jussi Isokuortti, Emma E. Comer, Sean T. Roberts*, Zachariah A. Page*

Department of Chemistry, The University of Texas at Austin, Austin, TX, 78712 USA

*Email: roberts@cm.utexas.edu

*Email: zpage@cm.utexas.edu

ABSTRACT

The rapid photochemical conversion of materials from liquid to solid (i.e., curing) has enabled the fabrication of modern plastics used in microelectronics, dentistry, and medicine. However, industrialized photocurables remain restricted to unimolecular bond homolysis reactions (Type I photoinitiations) that are driven by high-energy UV light. This narrow mechanistic scope both challenges the production of high-resolution objects and restricts the materials that can be produced using emergent manufacturing technologies (e.g., 3D printing). Herein, we develop a photosystem based on triplet-triplet annihilation upconversion (TTA-UC) that efficiently drives a Type I photocuring process using green light at low power density ($<10 \text{ mW/cm}^2$) and in the presence of ambient oxygen. This system also exhibits a superlinear dependence of its cure depth on light exposure intensity, which enhances spatial resolution. This enables for the first-time integration of TTA-UC in an inexpensive, rapid, and high-resolution manufacturing process, digital light processing (DLP) 3D printing. Moreover, relative to traditional Type I and Type II (photoredox) strategies, the present TTA-UC photoinitiation method results in improved cure depth confinement and resin shelf-stability. This report provides a user-friendly avenue to utilize TTA-UC in ambient photochemical processes and paves the way towards fabrication of next generation plastics with improved geometric precision and functionality.

INTRODUCTION

Light-driven polymerizations have enabled transformative advances in materials chemistry from coatings, adhesives, and lithography used in the fabrication of modern microelectronics to emergent additive manufacturing technologies (e.g., 3D printing) used broadly in the dental and medical industries to create items ranging from teeth alignment devices to surgical tools.¹⁻³ Vat-based photopolymerizations wherein rapid (\sim seconds) solidification of liquid resin occurs upon exposure to light (i.e., photocuring) has led to some of the highest build rates of any 3D printing technique. Moreover, the precise spatial and temporal control offered by light has resulted in unparalleled print fidelity (i.e., feature resolution).⁴⁻⁹ Despite these impressive achievements, several challenges in light-based 3D printing persist. This includes a reliance on high-energy photons ($<400 \text{ nm}$, UV) and/or high light exposure intensity ($>100 \text{ mW/cm}^2$), the need for inert printing conditions (e.g., N_2 or Ar atmosphere), and the high cost of printing components (e.g., pulsed lasers) (**Fig. 1**). These issues limit both accessibility, owing to high cost, and materials scope due to photodegradation and shallow penetration depth that arises from non-specific absorption and scattering of short-wavelength, UV light.^{8,10}

In recent years, various strategies have been developed to address the particular issue of UV photocuring. This includes photocatalysts that directly operate using visible and near-infrared light¹¹⁻¹⁶ as well as more sophisticated multiphoton excitation modes for catalysts that require higher energy, such as two-photon absorption,¹⁷ two-step absorption,¹⁸ and photon upconversion^{19,20}. Notably, the latter three techniques have an inherent quadratic relationship between incident light intensity and photocuring rate. This superlinear relationship stems from the requisite combination of multiple photons to generate the radical species that initiate polymerization. In turn, photocuring can be accomplished within a focal point of light, which has allowed production of sub-diffraction limited features (roughly $\lambda/2$) and voxel-by-voxel (i.e., volumetric) 3D printing.²¹ However, to-date 3D printing in this manner has required scanning a high-intensity, tightly-focused laser beam ($>1 \text{ W/cm}^2$), which is expensive (\sim \\$10k-100k instrumentation) and results in slow fabrication ($<10^{-3} \text{ mm}^3/\text{s}$) of objects confined to small volumes.²¹

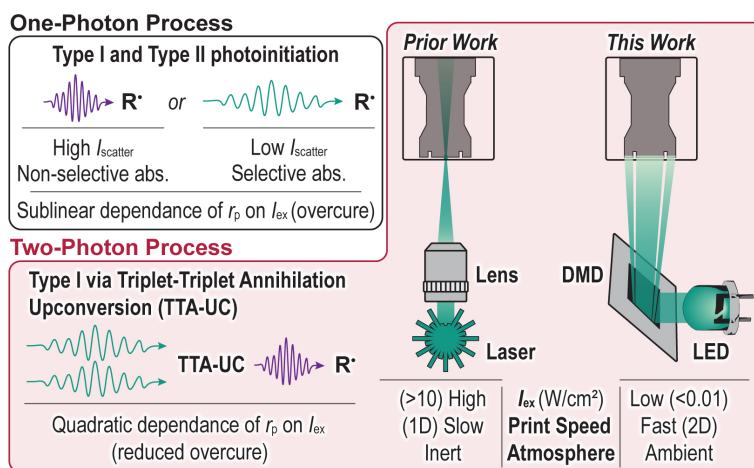


Figure 1. Previous work based on one- and two-photon stereolithographic methods vs. this work applying TTA-UC for two-photon digital light processing 3D printing. I_{scatter} , scattered light intensity; abs., absorbance; r_p , rate of polymerization; I_{ex} , excitation intensity.

As an alternative 3D printing strategy to multiphoton laser-based methods, digital light processing (DLP) offers a low-cost route (~\$1k instrumentation) to the rapid fabrication (~1 mm³/s) of large volume objects.²¹ DLP 3D printing operates in a layer-by-layer fashion, where each exposure represents a 2D projection (i.e., slice) of the 3D object (**Fig. 1**).²² Typical projection intensities in commercial DLP 3D printers range from ~5-50 mW/cm². However, higher intensity light engines (>100 mW/cm²) represent an active area of research given the potential for faster production speeds that offset the additional energetic costs. Although the feature resolution of DLP 3D printing at present does not match multiphoton techniques, it can provide fidelity on the ~10-100 μm scale with proper optimization. Specifically, feature optimization is accomplished by mitigating lateral (x,y) and vertical (z) overcure, (i.e., solidification that occurs outside the defined irradiation zones). However, speed and resolution are often at odds within one-photon systems given that high light sensitivity is required to achieve rapid photocuring. Thus, scattered light and vertically transmitted light beyond a single layer often result in overcure, reducing feature fidelity.

Relative to standard DLP 3D printing, a multiphoton method has the potential to improve resolution, as the scattered, and through-slice transmitted light lacks the intensity to induce curing given the superlinear dependence of polymerization rate on excitation power. Of the aforementioned multiphoton excitation pathways, triplet-triplet annihilation upconversion (TTA-UC) stands out due to its capability to operate efficiently (>10% quantum yield) under DLP-relevant, low-intensity excitation (<50 mW/cm²).²³ Indeed, TTA-UC-driven polymerizations have garnered considerable attention in recent years²⁴⁻³¹ but they have yet to be applied to DLP 3D printing. Instead, TTA-UC photocuring has recently been used for volumetric 3D printing. For example, Congreve and coworkers confined a TTA-UC system into silica-coated nanocapsules that were dispersed in a resin to print centimeter-scale objects³² while Hayward and coworkers directly dissolved TTA-UC dyes into a resin for microscale fabrication using a focused LED source.³³ However, despite these demonstrations, TTA-UC 3D printing has remained limited to high-intensity excitation (>10 W/cm²) and stringent oxygen-free conditions.³²⁻³⁵

Herein, our objective was to make upconversion-based 3D-printing more accessible by constructing a TTA-UC-driven photopolymerization system that achieves the desired superlinear (~quadratic) intensity dependence (and hence high spatial resolution) upon exposure to low-intensity (<10 mW/cm²) visible light from an inexpensive LED source under ambient conditions. To accomplish this objective, we have developed a TTA-UC to Type I photoinitiation system through systematic resin formulation optimization and characterization. We also providing direct comparisons of the optimized TTA-UC resin to state-of-the-art Type I and Type II photoinitiation systems. Following optimization, the TTA-UC to Type I photosystem provides short gelation times (<60 seconds) with low-intensity green light exposure in the presence of ambient oxygen, which is competitive with Type II photosystems. With this resin formulation, we demonstrate for the first time the utility of TTA-UC in DLP-based 3D printing using

a green LED to rapidly produce high-resolution objects (~ 100 μm scale features). This showcases the potential for TTA-UC systems to provide a commercially-viable platform for inexpensive light-based manufacturing.

RESULTS AND DISCUSSION

The photopolymerization system designed here couples two distinct processes, TTA-UC and Type I photoinitiation (i.e., unimolecular bond homolysis post-excitation) (Fig. 2, red boxes). The TTA-UC cascade begins with absorption of a low-energy (~ 525 nm, green light) photon by the photosensitizer (PS), platinum octaethylporphyrin (PtOEP). The resultant spin-singlet excited state ($^1[\text{PS}]^*$) of PtOEP then undergoes rapid intersystem crossing (ISC) to a long-lived spin-triplet excited state ($^3[\text{PS}]^*$). Next, this photoexcitation is transferred to 9,10-diphenylanthracene (DPA), a common annihilator (An) whose lower triplet energy relative to PtOEP ($E_{T,\text{PtOEP}} = 1.91$ eV, (Fig. S6); $E_{T,\text{DPA}} = 1.77$ eV)³⁶ enables triplet energy transfer (TET) between these compounds. Triplet-triplet annihilation (TTA) can then proceed when two annihilators in their triplet excited state, $^3[\text{An}]^*$, collide, yielding one ground state annihilator, $^1[\text{An}]$, and one annihilator in its singlet excited state, $^1[\text{An}]^*$. The excited spin-singlet annihilator can then emit a high-energy photon (~ 420 - 440 nm, violet-blue light, Fig. S7) that can be absorbed by phenylbis(2,4,6-trimethylbenzoyl)phosphine oxide (BAPO, Fig. S8), an efficient Type I photoinitiator that does not absorb the low-energy green photons emitted by the LED (Fig. S9) being used to excite PtOEP. In addition to emission-reabsorption, BAPO can be activated via energy transfer from $^1[\text{An}]^*$. In either case, the excited initiator ($^1[\text{I}]^*$) will cleave in a homolytic fashion to yield two radicals capable of initiating polymerization.

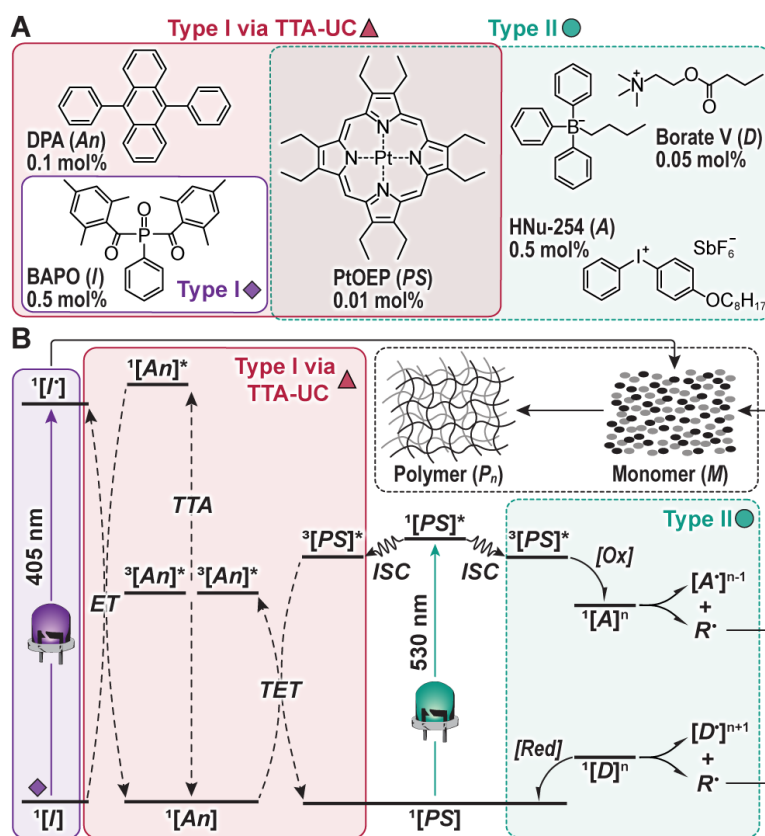


Figure 2. Photosystem components and photoinitiation mechanisms. (A) Chemical structures for Type I (left, violet), TTA-UC (center, red), and Type II (right, green) photosystems used in this study. **PS**, photosensitizer, platinum octaethylporphyrin (PtOEP); **An**, annihilator, diphenylanthracene (DPA); **I**, initiator, bisacylphosphine oxide (BAPO); **A**, electron acceptor, 4-octyloxydiphenyliodonium hexafluoroantimonate; **D**, electron donor, butrylcholine butyltriphenylborate. (B) Energy level schematic showing the mechanisms for photoinitiation. Processes include photoexcitation, intersystem crossing (ISC), electron transfer (solid hook arrows), and energy transfer (dashed arrows). TET, triplet energy transfer; TTA, triplet-triplet annihilation; [Ox], oxidation; [Red], reduction; R \cdot , radical; M, monomer; P $_n$, polymer.

As a benchmark, this process was directly compared with an analogous Type II photopolymerization system driven by green light (**Fig. 2**, green boxes). In this photosystem, PtOEP serves as a photoredox catalyst (labelled for simplicity as **PS**), while diphenyliodonium and *n*-butyl triphenylborate salts serve, respectively, as electron acceptor (**A**) and donor (**D**) components, completing an efficient redox cycle where radicals are generated on both ends. In addition, polymerizations driven via direct photoexcitation (~405 nm, UV-violet light, Fig. S9) of the Type I photoinitiator, BAPO, served as controls (**Fig. 2**, violet boxes).

Several acrylate monomers were initially screened with the TTA-UC system, namely isobornyl acrylate, dimethyl acrylamide, carbitol acrylate, and 2-phenoxyethyl acrylate (PhOEA). Of these four monomers, 2-phenoxyethyl acrylate provided the best combination of solubility and polymerization rate (Fig. S10, Table S1) and was therefore used for all further photo-physical and polymerization studies. Notably, although uncommon in photocurable resins, 2-phenoxyethyl acrylate is an inexpensive monomer (as low as ~\$50/kg) derived from the commodity chemical phenoxyethanol,³⁷ making it of viable utility in commercial additive manufacturing.

As a first step towards TTA-UC-based photopolymerization, we characterized the upconversion quantum efficiency (Φ_{UC}) and intensity threshold (I_{th}) of the PtOEP/DPA TTA-UC system via photoluminescence spectroscopy under an inert nitrogen atmosphere. To preclude DPA fluorescence quenching, measurements were performed in the absence of BAPO (i.e., using only PtOEP and DPA). To match the polymerization conditions described later, PtOEP and DPA were dissolved in 2-phenoxyethylacrylate at a concentration of 0.6 and 6 mM, respectively. Exposure of this mixture to 50 mW/cm² 532 nm green laser light resulted in no observable DPA fluorescence (**Fig. 3A**) despite prior reports of TTA-UC occurring for PtOEP/DPA mixtures at <50 mW/cm², albeit in more traditional solvents (e.g., toluene).³⁸ Increasing the excitation intensity (I_{ex}) to 1000 mW/cm² resulted in DPA fluorescence monitored at 436 nm that grew in intensity during the first ~30 seconds of exposure. After ~60 seconds the DPA fluorescence decreased, concomitant with the appearance of a red emission band centered at ~645 nm that was attributed to PtOEP phosphorescence. Upon concluding the experiment, the formation of solid inside the cuvette at the position of irradiation was observed, indicating that the PtOEP/DPA TTA-UC system can initiate photopolymerization in the absence of BAPO, although it requires high I_{ex} and exposure times (Fig. S11). In the case of DPA, the energy of ¹[**An**]* is too low to initiate acrylate polymerization, which was confirmed experimentally through direct excitation of DPA in monomer (Fig. S12). As such, an alternate initiation pathway within the TTA-UC photosystem must exist, which we speculate could occur via electron transfer to monomer from a high-energy coupled triplet pair state that forms upon TTA³⁹⁻⁴¹ prior to ¹[**An**]*.

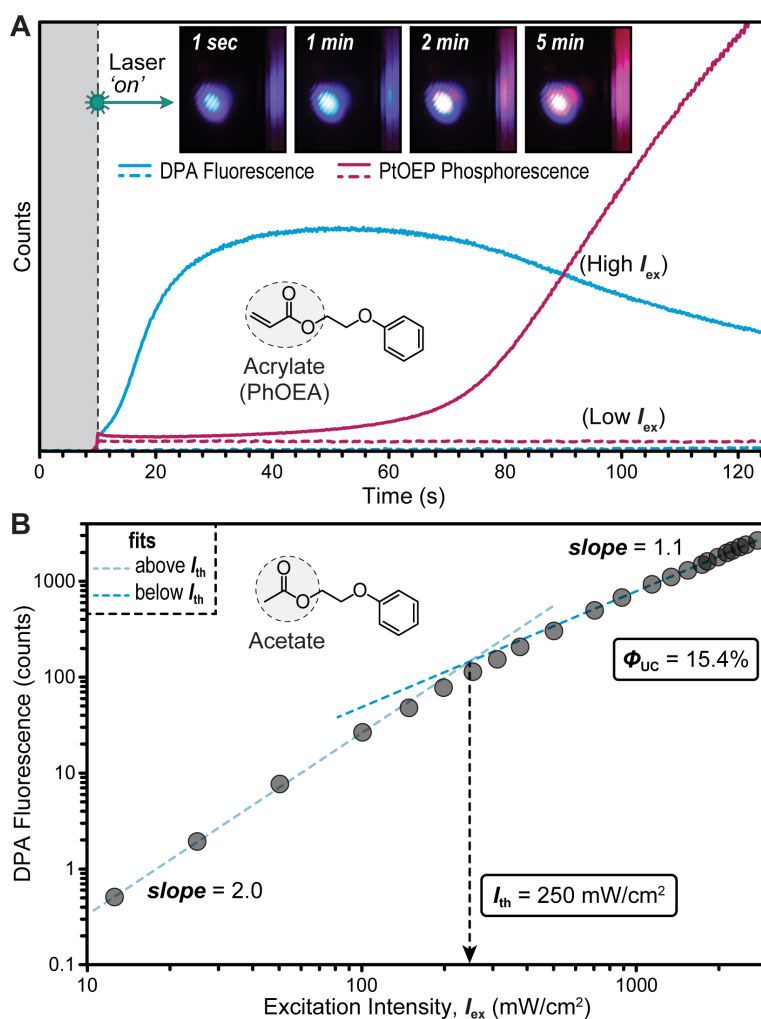


Figure 3. Characterization of PtOEP/DPA TTA-UC under an inert atmosphere using photoluminescence spectroscopy upon green (532 nm) laser excitation. (A) Time evolution of upconverted DPA fluorescence (cyan) and PtOEP phosphorescence (maroon) in 2-phenoxyethylacrylate monomer. Photoluminescence was measured at 436 nm and 645 nm at low and high excitation intensity ($I_{\text{ex}} = 50$ and 1000 mW/cm^2). (B) Upconverted DPA fluorescence in 2-phenoxyethylacetate as a function of excitation intensity used to quantify the threshold intensity (I_{th}) using a double-logarithmic plot.

The time-evolution of emission from the TTA-UC system (**Fig. 3A**) was attributed to photoinduced electron transfer from DPA to acrylate, which was recently shown to be a viable initiation mechanism for photopolymerization.²⁵ We hypothesize that upon light exposure, upconverted fluorescence quenching by 2-phenoxyethylacrylate occurs, leading to the weak TTA-UC observed. Over time, the local concentration of monomer, acting as a DPA quencher, decreases due to polymerization, leading to a slow gain in DPA fluorescence with continued light exposure. Eventually however, polymerization increases the viscosity of the solution to a point that diffusion-based TET from PtOEP to DPA and TTA between triplet excited DPA ($^3[\text{An}]^*$) molecules is severely hindered, leading to a decrease in DPA fluorescence and increase in PtOEP phosphorescence. Notably, the changes in photoluminescence from blue to red emission are visible to the naked eye, providing visual cues that uniquely enable qualitative tracking of this process (Fig. S13, Video S1).

Although the time-dependent emission behavior observed in 2-phenoxyethylacrylate was unique, DPA quenching by the monomer precluded us from quantitatively determining Φ_{UC} and I_{th} for the PtOEP/DPA TTA-UC system. To bypass this issue, 2-phenoxyethylacrylate was replaced with an analogous non-polymerizable solvent, 2-phenoxyethylacetate. Using the same concentrations of PtOEP (0.6 mM) and DPA (6 mM) as that used for

photopolymerization (described below), the DPA fluorescence intensity at 436 nm was tracked as a function of 532 nm I_{ex} (**Fig. 3B**). Plotting the results on a log-log scale revealed a change in slope from ~ 2 to 1 at $I_{\text{ex}} \approx 250 \text{ mW/cm}^2$, which identifies I_{th} . Below I_{th} , spontaneous decay of $^3[\text{An}]^*$ is rate-limiting, whereas above I_{th} TTA becomes the dominant, and thus rate-limiting pathway.²³ This behavior for TTA-UC systems can be described using equation (1):⁴²

$$I_{\text{th}} = \frac{2(k_{\text{An}}^{\text{T}})^2}{\alpha\phi_{\text{TET}}\gamma_{\text{TTA}}} \quad (\text{Eq. 1})$$

where k_{An}^{T} is the $^3[\text{An}]^*$ decay rate constant, α is the PS absorption coefficient, ϕ_{TET} is the TET efficiency from the $^3[\text{PS}]^*$ to the $^1[\text{An}]$, and γ_{TTA} is the TTA second-order rate constant.

To estimate I_{th} in acrylate relative to the acetate (proxy) solvent, each component of equation 1 was systematically characterized apart from γ_{TTA} , which was assumed to be similar in both solvents as the decay of upconverted fluorescence in the acrylate cannot be reliably measured. Under equimolar conditions that provide high optical densities, α is similar in both acrylate and acetate. To characterize ϕ_{TET} in each solvent, time-resolved photoluminescence spectroscopy under an inert nitrogen atmosphere was used to measure changes in the PtOEP phosphorescence lifetime due to quenching by DPA (Fig. S14-S17 and Table S2). In the absence of DPA, the lifetime of PtOEP was found to be ~ 79 and $\sim 52 \mu\text{s}$ in acrylate and acetate solvents, respectively. The addition of 6 mM DPA to each solution decreases these values to $\sim 1.9 \mu\text{s}$ for both solvents, indicating that ϕ_{TET} is $>96\%$. Finally, k_{An}^{T} values were extracted using transient absorption spectroscopy by monitoring the decay of an induced absorption signal from $^3[\text{An}]^*$ at 475 nm⁴³ (Fig. S18-S19 and Table S2), which yielded lifetimes of $159 \mu\text{s}$ ($k_{\text{An}}^{\text{T}} \approx 6,300 \text{ s}^{-1}$) and $36 \mu\text{s}$ ($k_{\text{An}}^{\text{T}} \approx 27,500 \text{ s}^{-1}$) in acrylate and acetate, respectively. Given the squared dependence of I_{th} on k_{An}^{T} (equation 1), we estimate that I_{th} is $\sim 13 \text{ mW/cm}^2$ in acrylate, which is $\sim 20\times$ lower relative to acetate. Thus, the TTA-UC system was anticipated to operate effectively under excitation intensities relevant to DLP 3D printing. Further supporting this expectation was the high maximum Φ_{UC} , which was measured as 15.4% in acetate, albeit at high I_{ex} values ($3,000 \text{ mW/cm}^2$) (Fig. S20). Notably this Φ_{UC} value is out of a maximum of 50% (theoretical TTA-UC limit) and is conservative given a lack of correction for inner filter effects. Despite the stark disparity in I_{th} when using acetate vs. acrylate solvents, we hypothesize that Φ_{UC} is comparable in each solvent given the governing factors provided in equation (2):⁴⁴

$$\Phi_{\text{UC}} = \frac{1}{2}\phi_{\text{ISC}}\phi_{\text{TET}}\phi_{\text{TTA}}f\phi_{\text{fl}} \quad (\text{Eq. 2})$$

where ϕ_{ISC} is the ISC efficiency of the PS (PtOEP), ϕ_{TTA} is the TTA quantum yield, f is the spin-statistical factor (i.e., the probability of forming an excited singlet state upon TTA⁴¹), and ϕ_{fl} is the An (DPA) fluorescence quantum yield. Given a common PS (PtOEP) that leverages spin-orbit coupling from the heavy Pt atom to drive ISC, ϕ_{ISC} was assumed to be similar in acrylate and acetate. As discussed previously, ϕ_{TET} is near unity in both systems due to the high An (DPA) concentration employed. Additionally, ϕ_{TTA} approaches unity at excitation intensities $\gg I_{\text{th}}$ irrespective of solvent⁴⁵. Finally, the effect of acrylate vs. acetate solvent on ϕ_{fl} was probed by characterizing the fluorescence lifetime (τ_{fl}) of DPA post 375 nm excitation (Fig. S21). A τ_{fl} value of 6.8 ns was found in both solvents, which is nearly identical to τ_{fl} in toluene (6.9 ns) where ϕ_{fl} is \sim unity.⁴⁶ This suggests that ϕ_{fl} should be similar and close to unity in both acetate and acrylate. Together, these results highlight that the present TTA-UC system operates efficiently with an uncorrected Φ_{UC} of 15.4% in acetate (compared to $\sim 18\text{-}26\%$ in other solvents)⁴⁷, while having a low estimated I_{th} of 13 mW/cm^2 in acrylate (compared to 15 mW/cm^2 in toluene⁴⁶).

Having characterized the upconversion system it was next employed to drive a classic Type I photopolymerization, using BAPO as the initiator (**I**) as its absorption spectrum shows good overlap with the emission spectrum of DPA (**Fig. 4A**). A standard green LED ($\lambda_{\text{max}} = 525 \text{ nm}$) was selected as the excitation light source as its emission profile overlapped well with the absorption profile of PtOEP used in both the TTA-UC and Type II photosystems, without being absorbed by BAPO. Additionally, the LED was equipped with a $525 \times 25 \text{ nm}$ bandpass (BP) filter to ensure selective absorption by PtOEP (Fig. S9).

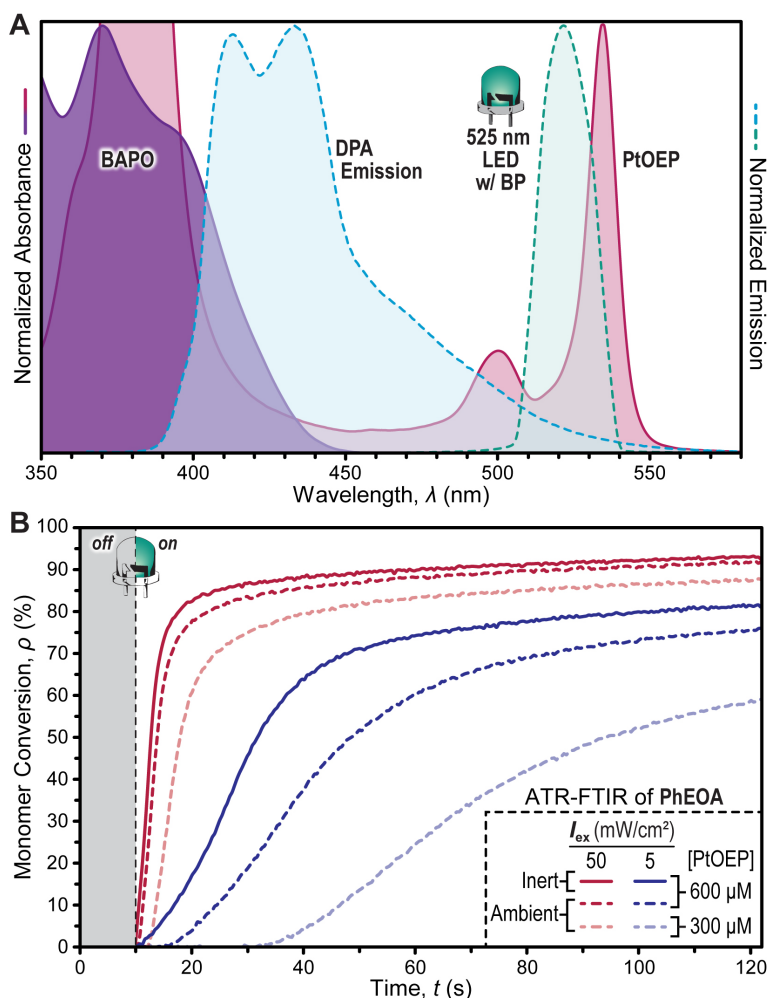


Figure 4. (A) The absorption spectrum of BAPO (purple shaded) overlaps with the emission spectrum of DPA (cyan dashed). Likewise, the absorption spectrum of PtOEP (red shaded) overlaps with the emission spectrum of the 525 nm LED used to excite the TTA-UC system. Note, the LED has been passed through a 525 \times 25 nm bandpass filter to narrow its spectrum. (B) FTIR-ATR, plotting C=C conversion vs time of the standard resin ([PtOEP] = 600 μ M; [DPA] = 6 mM; [BAPO] = 30 mM) and its 1/2 dilution. Resins were tested under inert (solid) and ambient (dashed) conditions; and high intensity (50 mW/cm², red) or low intensity (5 mW/cm², blue) 525 nm light irradiation.

Initial resin formulation optimization focused on maximizing the rate of polymerization (r_p) by adjusting photosystem component concentrations. Real-time Fourier transform infrared (RT-FTIR) spectroscopy performed in an attenuated total reflectance (ATR) configuration was used to quantify r_p by measuring the conversion of monomer to polymer (ρ) via loss of the monomer C=C stretching band at 808 cm⁻¹.⁴⁸ Optimization via RT-FTIR kinetics led to a resin consisting of 0.01 mol% (~600 μ M) PtOEP, 0.1 mol% DPA, and 0.5 mol% BAPO, a **PS:An:I** ratio of 1:10:50 (Fig. S22-S23). The **PS:An** ratio in this system is similar to that used for upconversion in soft materials,⁴⁹ while the **I** concentration corresponds to 1 wt% in the resin formulation, which is within the standard range of Type I photoinitiators used in photocurable resins (~0.5-5 wt%).^{10,14} This **I** concentration falls at the lower end of the commercial use range, which has the added potential benefit of improving resin stability to accidental ambient light exposure.

Photopolymerizations with the optimized formulation were conducted using I_{ex} values of 5 and 50 mW/cm² under both ambient and inert (argon) atmospheric conditions. In the absence of oxygen, excellent temporal control was observed, where polymerization began right after turning the LED 'on' (Fig. 4B). The r_p , measured as the initial

slope of monomer C=C conversion, was 109 ± 6.4 mM/s and 901 ± 41 mM/s for I_{ex} values of 5 and 50 mW/cm², respectively (**Fig. 4B** and Table S3) under inert conditions. As a control, resins without **An** (i.e., only **PS** and **I** present) did not polymerize upon exposure to the 525 nm LED (50 mW/cm²) (Fig. S24). In contrast, under the same excitation conditions (525 nm LED, 50 mW/cm²) control resins without **I** (i.e., only **PS** and **An** present) showed a very slow polymerization ($r_p = 5.3 \pm 0.5$ mM/s) (Fig. S25), consistent with the aforementioned solid formation observed during Φ_{UC} characterization (Fig. S11). Also of note, a red-shifted Type I acylgermane initiator (Ivocerin®) was examined to increase the absorption overlap with upconverted DPA fluorescence (Fig. S8). However, only modest improvements in r_p ($\leq 15\%$ increase) were measured relative to analogous resins with BAPO (Fig. S26 and Table S4). Returning to the TTA-UC photosystem containing BAPO, the maximum C=C conversion (ρ_{max}) was $82 \pm 2\%$ and $93 \pm 1\%$ for the I_{ex} of 5 and 50 mW/cm², respectively (**Fig. 4B** and Table S3). The incomplete C=C conversion was attributed to the increase in viscosity upon polymerization, which hinders diffusion-limited processes. Notably, the 11% larger ρ_{max} observed when using the higher I_{ex} may be rationalized by the larger r_p and concomitant heat released from the exothermic reaction propagation, which can facilitate diffusion and thereby higher conversion.

Irradiating the same mixtures under ambient conditions resulted in a r_p of 85 ± 7 mM/s and a ρ_{max} of $75 \pm 1\%$ for an I_{ex} of 5 mW/cm², while increasing I_{ex} by a factor of 10, to 50 mW/cm², boosted these values to $r_p = 834 \pm 34$ mM/s and $\rho_{\text{max}} = 92 \pm 1\%$ (**Fig. 4B** and Table S3). Notably, the r_p at 50 mW/cm² under ambient conditions was only 7% smaller than under inert conditions. This apparent low sensitivity to oxygen is attributed to triplet quenching rates that outcompete the rate of oxygen diffusion facilitated by the high **PS** concentration (~ 600 μM), despite the relatively low viscosity (η) of the photopolymerizable resin ($\eta_{\text{monomer}} \approx 11$ mPa·s), which was expected to enhance oxygen quenching. To the best of our knowledge, the low oxygen sensitivity is unprecedented for TTA-UC and provides a key avenue towards commercial additive manufacturing that is predominantly accomplished under ambient conditions. The effect of oxygen however is more apparent at an I_{ex} of 5 mW/cm², where an inhibition time (t_{inh}) (i.e., period of no conversion after light ‘on’) of ~ 4 s emerges (**Fig. 4B**). The t_{inh} likely corresponds with the time it takes to fully consume oxygen in the irradiation zone. This effect was further pronounced upon diluting the photosystem to 1/2 (i.e., 300 μM PtOEP, **Fig. 4B**) and 1/10 (i.e., 60 μM PtOEP, Fig. S27-S30 and Table S5) of the original formulation. At 1/2 the original concentration under ambient conditions, the r_p was 56 ± 3 mM/s, ρ_{max} was $59 \pm 2\%$, and t_{inh} was 21 ± 1 s for an I_{ex} of 5 mW/cm². Increasing I_{ex} to 50 mW/cm² heightened these values to $r_p = 504 \pm 25$ mM/s, $\rho_{\text{max}} = 87 \pm 1\%$, and $t_{\text{inh}} = 2.0 \pm 0.2$ s under ambient conditions.

Given the large apparent influence of I_{ex} on the photopolymerization kinetics, we characterized its impact on the behavior of the optimized TTA-UC resin (**Fig. 5A**). Samples were measured under an inert atmosphere to allow intrinsic TTA-UC characteristics, such as I_{th} and r_p , to be quantified in the absence of oxygen inhibition. I_{ex} was varied by more than three orders of magnitude, from 0.1 mW/cm² to 200 mW/cm². This resulted in r_p values ranging over 4 orders of magnitude, from 0.11 ± 0.01 mM/s to 2200 ± 150 mM/s. Plotting r_p vs. I_{ex} on a double logarithmic scale revealed two linear regimes with distinct slopes that converge at $I_{\text{ex}} \approx 4$ mW/cm² (**Fig. 5B**, Fig. S31-33 and Table S6). In the low I_{ex} region (< 4 mW/cm²), the slope is superlinear (1.95 ± 0.03), which is characteristic of initiation occurring through a two-photon process (i.e., TTA).^{33,50} In the high I_{ex} region (> 4 mW/cm²), the slope becomes sublinear (0.66 ± 0.04), which is close to the expected slope of 0.5 for one-photon initiated polymerizations that operate under conventional bimolecular termination events (i.e., $r_p \propto I_{\text{ex}}^{1/2}$)^{51,52}. The observable trends of I_{ex} on polymerization kinetics are analogous to that observed for upconverted photoluminescence via the TTA mechanism. Moreover, the two fitted slopes intersect at ~ 4 mW/cm², which is within the same order of magnitude as the estimated I_{th} value of 13 mW/cm² from equation 1. Taken together, these results suggest that monitoring r_p as a function of I_{ex} provides an effective method to experimentally determine I_{th} for photopolymerizations driven by a two-photon process.

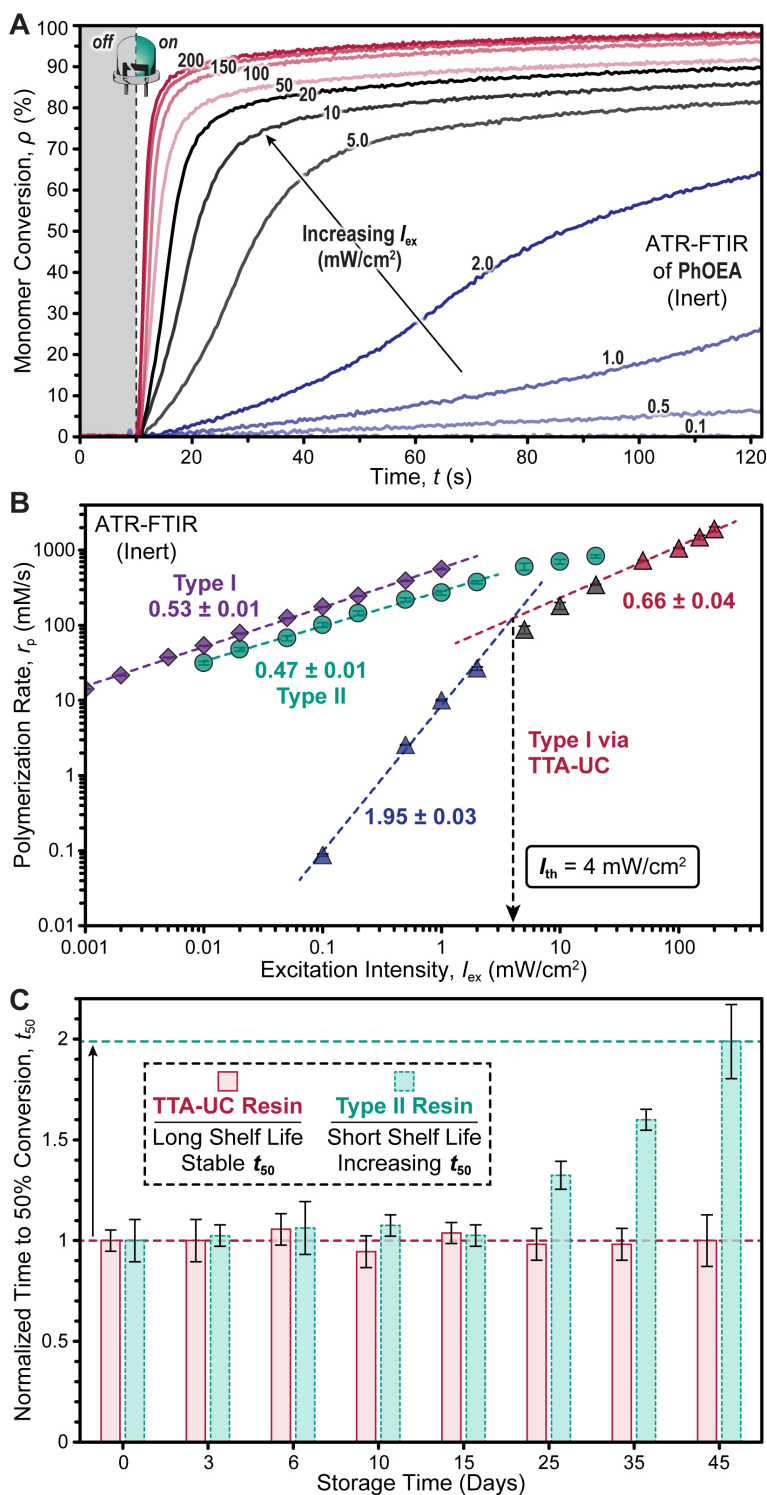


Figure 5. (A) FTIR-ATR intensity sweeps of the TTA-UC resin in 2-phenoxyethylacrylate (PhOEA) under an argon atmosphere with the optimized photosystem ($[PtOEP] = 0.6$ mM; $[DPA] = 6$ mM; $[BAPO] = 30$ mM). The 525 nm LED was turned on at 10 s. (B) Plot of initial photopolymerization rate vs. light intensity for the Type I photosystem driven by TTA-UC (triangles), Type I photosystem driven by direct UV/violet excitation of BAPO (diamonds), and the Type II photosystem (circles). The number near each linear best fit curve indicates its slope. (C) Normalized time to reach 50% conversion (t_{50}) of the Type II and TTA-UC resins over 45 days.

To confirm that the superlinear behavior was unique to TTA-UC based Type I photopolymerizations, r_p values for the PtOEP/DPA/BAPO system were compared with those obtained by direct excitation of the benchmark Type I and Type II photosystems detailed in **Fig. 1 (Fig. 5B)**. For the Type I photopolymerization, BAPO was employed as the photoinitiator at an equimolar concentration (30 mM) to that used in the optimized TTA-UC formulation and was photoexcited using a 405 nm UV/violet LED whose output was tuned to provide I_{ex} values from 0.001-1 mW/cm². Likewise, Type II photopolymerizations were performed using an equimolar concentration of PtOEP (600 μ M) to that employed in the optimized TTA-UC formulation, along with 50 and 5 equivalents (30 and 3 mM, respectively) of diphenyliodonium and *n*-butyl triphenylborate salts as the electron acceptor and donor, respectively. The same 525 nm LED with a 525 \times 25 nm bandpass filter used for the TTA-UC resin was again employed for the Type II photosystem, with I_{ex} values employed ranging from 0.01 to 20 mW/cm² to provide comparable r_p values.

Examining the performance of the Type I photosystem as a function of I_{ex} revealed r_p values from 17.3 ± 1.1 mM/s to 679 ± 2.0 mM/s and a sublinear relationship (slope = 0.53 ± 0.01) over the full range of r_p values when plotting on a double logarithmic scale (**Fig. 5B**, Fig. S34-S35 and Table S7). Similarly, the Type II system yields r_p values that display a sublinear dependence on I_{ex} (slope = 0.47 ± 0.01), which becomes even more pronounced (slope < 0.3) at higher excitation intensities due to undesirable side reactions (**Fig. 5B**, Fig. S36-S39 and Table S7). Although direct activation of both the Type I and Type II resins provided high r_p 's at low I_{ex} 's, the sublinear relationship between the two is expected to limit spatial resolution by facilitating overcure from scattered light and light transmitted beyond the depth of a single layer in the case of DLP (or other layer-by-layer) 3D printing. In contrast, the TTA-UC based mechanism is anticipated to enhance spatial resolution given that scattered light and light transmitted through a layer can be tuned to fall below I_{th} where a superlinear relationship between r_p and I_{ex} exists.

Relevant to the translation of photocurable resins from lab to market is their stability. To this end, a TTA-UC resin with the optimal formulation was prepared, stored under ambient conditions (i.e., room temperature, atmospheric air, and in the dark), and tested using RT-FTIR periodically over the course of 45 days (**Fig. 5C**, Fig. S40). Notably, little-to-no change in the photopolymerization kinetics, nor starting C=C absorption was observed, indicating excellent stability. In contrast, the analogous Type II resin containing PtOEP as the photoredox catalyst showed a steady increase in time to reach 50% conversion (t_{50}) over the same timeframe, ultimately resulting in a $2\times$ increase in t_{50} after 45 days (**Fig. 5C**, Fig. S41). This result showcases the potential for visible light reactive resins that undergo TTA-UC to Type I photoinitiation to be bottled and stored long term for 3D printing applications.

To make the TTA-UC resin compatible with DLP 3D printing, we next incorporated trimethylolpropane triacrylate (TMPTA) as a crosslinker in a 1:1 weight ratio with 2-phenoxyethyl acrylate. Characterization of this resin was accomplished using transmission-mode RT-FTIR and photorheology for thin-films (100 μ m) under an ambient oxygen atmosphere to mimic layer curing in DLP 3D printing. Using the green LED with an I_{ex} of 10 mW/cm², RT-FTIR of the crosslinkable resin formulation revealed an r_p of 100 ± 3.1 mM/s (Fig. S42), which was within the same order of magnitude as the resin without crosslinker as measured using an ATR configuration, despite the presence of oxygen. Notably, polymerizations began shortly after turning the light on, with an average delay (t_{inh}) of 4.0 ± 0.5 s. This short inhibition period was presumed to arise from triplet quenching by oxygen, and it could be further reduced upon increasing I_{ex} from 10 to 50 mW/cm² (Fig. S42). This was also supported by decreasing the concentration of BAPO, which led to slower polymerization rates, but only a slight increase in t_{inh} (Fig. S43-S44). Furthermore, characterizing r_p for this system (100 μ m thickness in ambient oxygen) at several different intensities revealed an I_{th} of ~ 44 mW/cm² (**Fig. 6A, 6B** and Table S8), which was an order or magnitude larger than that measured using ATR under inert atmospheric conditions ($I_{th} = 4$ mW/cm²) and the theoretical value ($I_{th} = 13$ mW/cm²). Among the intensities measured, an $I_{ex} = 7$ mW/cm² matched that used for 3D printing, which gave an r_p of 48 ± 1.3 mM/s and t_{inh} of 21 ± 0.3 s. Using these same conditions ($I_{ex} = 7$ mW/cm², thickness = 100 μ m), photorheology was used to estimate the minimum irradiation time required for curing (i.e., gel point), which was characterized by the crossover of storage (G') and loss (G'') moduli. Under these conditions, the average gel point was 39.6 ± 2.4 s (Fig. S45), which is within a reasonable timeframe for DLP 3D printing.

Expanding upon these initial photocuring results, a series of systematic photorheology experiments were performed to understand the influence of photopolymerization mechanism (TTA-UC, Type I, and Type II) on vertical (z) overcure (**Fig. 6C**, Fig. S46 and Table S9). To this end, a series of cure depth (C_d) experiments going beyond a single desired 100 μ m layer were performed, holding constant (to the best of our ability) key factors influencing C_d outside the photosystem composition and associated mechanism. Specifically, I_{ex} from the 405 nm LED for Type I

and 525 nm LED for Type II and TTA-UC was set to 0.1, 0.5, and 10 mW/cm², respectively, to provide similar r_p values of ~220 mM/s, as measured using RT-FTIR (Fig. S47). Furthermore, the 405 and 525 nm light-absorbing components (i.e., BAPO and PtOEP, respectively) provided resins with corresponding average LED transmittance values for a 100 μ m pathlength of 78% and 79%, respectively, across the full wavelength range of spectral overlap (i.e., considering chromophore absorbance and LED emission (Fig. S48-S50 and *optical density matching* section in the SI for more details). The C_d values were characterized as a function of light exposure time for each resin. After irradiation of the resin sitting in a 500 μ m gap between static parallel plates, unreacted monomer was wicked away and the upper plate was lowered stepwise (1 μ m/s) until reaching a set force of 2 N,⁵³ upon which the gap height was equated to C_d (Fig. 6C). Next, intrinsic resin properties influencing C_d were determined using the Jacobs' equation (3):⁵⁴

$$C_d = D_p \ln \left(\frac{E_0}{E_c} \right) \quad (\text{Eq. 3})$$

where D_p corresponds to the penetration depth of light, E_c is the critical exposure energy required to cure an infinitesimal layer, and E_0 is the experimental exposure energy (i.e., light dosage).^{53,55,56}

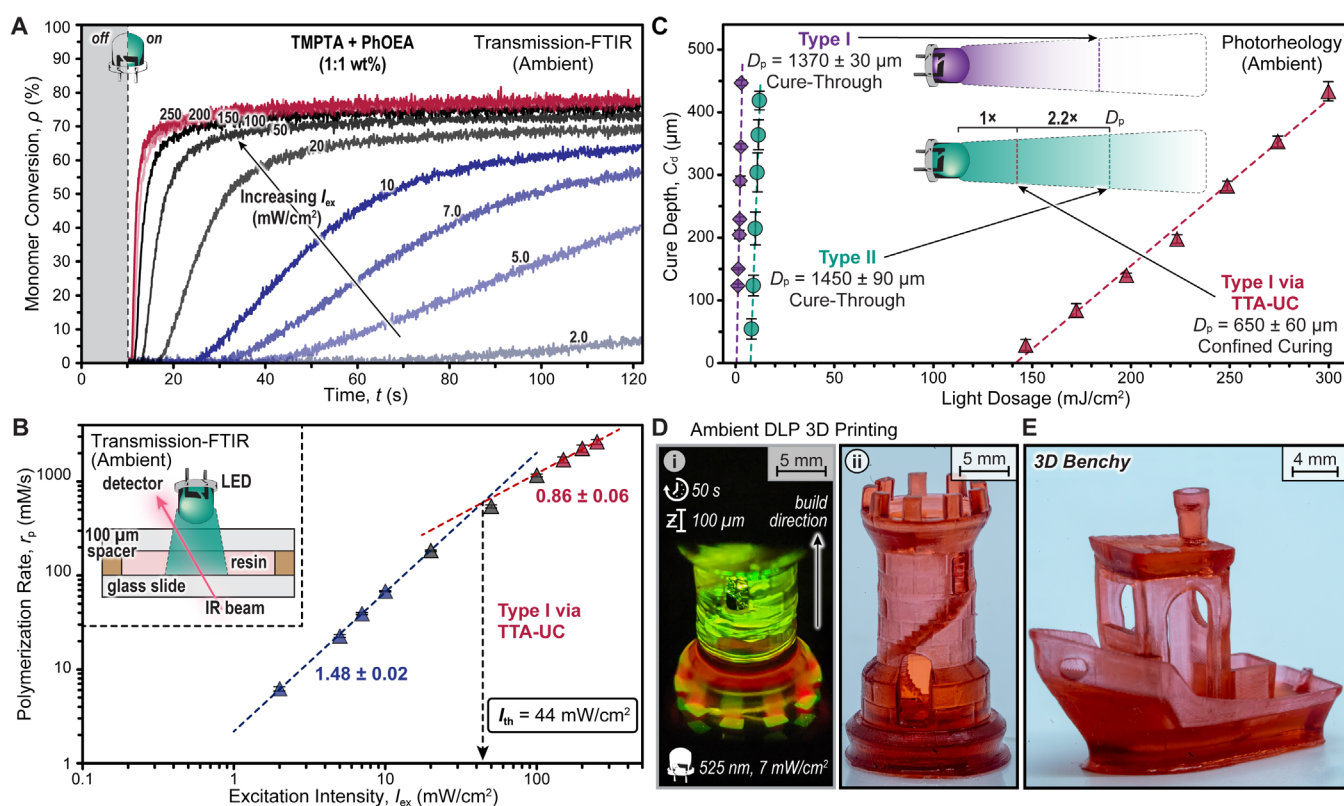


Figure 6. Testing of photocurable resins comprising trimethylolpropane triacrylate (TMPTA) and 2-phenoxyethylacrylate (PhOEA) (1:1 wt%) under an ambient oxygen atmosphere with the optimized photosystem ([PtOEP] = 0.6 mM; [DPA] = 6 mM; [BAPO] = 30 mM). (A) FTIR-ATR intensity sweeps using the 525 nm LED turned on at 10 s. (B) Plot of initial photopolymerization rate (mM/s) vs light intensity (mW/cm²) for the Type I photosystem driven by TTA-UC. The number near each linear best fit curve indicates its slope. (C) Cure depth as a function of light dosage (mJ/cm²) for the three resins. Critical exposure (E_c) and depth of penetration (D_p) values were determined from the semilog plot of C_d vs E_0 in Fig. S46. (D) Digital light processing (DLP) 3D printing under an ambient oxygen atmosphere of a Rook. (i) Active printing using a 525 nm LED, slice time of 50 seconds, and layer thickness of 100 μ m followed by (ii) the completed print. (E) DLP 3D printed Benchy, using the same conditions as for the Rook.

Plotting C_d vs. E_0 for each of the three resin formulations revealed a stark disparity in the light dosage required to cure a given depth (= slope) and the critical exposure, E_c (= x-intercept) for TTA-UC relative to the Type I and Type II controls (**Fig. 6C** and Fig. S46). Due to its lower quantum efficiency of initiation, TTA-UC driven Type I has an E_c that is $\sim 20\times$ higher than that of the Type I and II systems. Importantly, however, despite the higher energy requirement for TTA-UC, its associated D_p of $650 \pm 60 \mu\text{m}$ is $\sim 2\times$ lower than for Type I ($1370 \pm 30 \mu\text{m}$) and Type II ($1450 \pm 90 \mu\text{m}$). Given the nearly matched optical densities for the 525 and 405 nm absorbing resins, one would anticipate equivalent D_p values of $\sim 900 \mu\text{m}$ based on equation (4):

$$D_p^{\text{predicted}} = \frac{\log(0.37)}{-\varepsilon_{\text{avg}} \times [\text{PS}]} \quad (\text{Eq. 4})$$

where ε_{avg} is the average molar absorptivity based on the overlap between the green LED emission and **PS** or violet LED emission and **I** absorption profiles (see *Optical Density Matching* section in the SI for more details). However, this equation was created to correlate D_p to C_d for traditional free-radical polymerizations, where a sublinear relationship between I_{ex} and photocuring exists. The considerably lower D_p for TTA-UC is hypothesized to arise from the superlinear relationship between I_{ex} and r_p . In-turn, this should correspond with reduced vertical overcure (i.e., cure-through) from light transmitted beyond a single print layer, while also providing a mechanism to reduce lateral overcure from scattered light. As such, improved resolution for layer-by-layer 3D printing relative to conventional one-photon curing processes are anticipated when using the TTA-UC to Type I resin.

As a final proof-of-concept, the TTA-UC photosystem was employed for DLP 3D printing under comparable conditions to that used for the aforementioned characterization: a green LED having a λ_{max} of 525 nm, full width at half maximum (FWHM) of 34 nm, and maximum I_{ex} of $7 \text{ mW}/\text{cm}^2$ (Fig. S51). Printing was performed under ambient conditions with no resin deoxygenation. An initial print file containing 12 discrete sections with preprogrammed light exposure times from 5 to 115 seconds per $100 \mu\text{m}$ layer was used to determine the optimal exposure time (Fig. S52). From this, it was found that a minimum exposure time of 45 seconds/ $100 \mu\text{m}$ layer was required to fabricate objects with lateral (x,y) features as small as $100 \mu\text{m}$, which corresponds to $\sim 4\text{-}5$ pixels on the projected image. Notably, there was little observable lateral overcure at exposure times >45 seconds, which may arise from the two-photon nature of the photocuring process. Using an exposure time of $50 \text{ s}/100 \mu\text{m}$ ($\sim 7 \text{ mm}/\text{hr}$), two complex prints containing several overhangs and small holes were targeted. Specifically, a Rook that contained an internal spiral staircase and a 3D Benchy with small ($\sim 4 \text{ mm}$ diameter) portholes on the hull and a hollow smokestack were printed (**Fig. 6B**). Moreover, none of the TTA-UC to Type I prints required incorporation of photostable opaquing agents to achieve high-resolution features (i.e., mitigate overcure), which simplifies the resin formulation and paves an avenue to semi-transparent and colorless objects with further optimization, such as lowering **PS** concentration and/or identifying bleachable **PSs**. These DLP 3D prints showcase the potential of TTA-UC to Type I photocuring as a new mechanism for rapid, low-intensity, and high-resolution manufacturing.

CONCLUDING REMARKS

A Type I photocurable resin driven by TTA-UC with low intensity ($\sim 10 \text{ mW}/\text{cm}^2$) green light ($\sim 525 \text{ nm}$) that operates under an ambient oxygen atmosphere was demonstrated for the first time, which enabled rapid, high-resolution DLP 3D printing. This advance was facilitated by the high upconversion quantum efficiency ($\sim 15\%$) and low upconversion threshold ($<50 \text{ mW}/\text{cm}^2$) of the resin's PtOEP/DPA components. Optimization of the resin formulation using RT-FTIR spectroscopy under an inert argon atmosphere revealed that a 1:10:50 ratio for PtOEP:DPA:BAPO, where $[\text{PtOEP}] = 600 \mu\text{M}$, gave a rapid polymerization ($\sim 100 \text{ mM}/\text{s}$) at low light intensity ($\sim 10 \text{ mW}/\text{cm}^2$). Importantly, the polymerization rate of the TTA-UC to Type I system exhibited a quadratic dependence on light intensity. This feature can enable improved spatial resolution in 3D printing over that achievable with analogous Type I and II photosystems by mitigating curing that occurs outside of the desired irradiation zone from low-intensity transmitted and scattered light. Further supporting translation to 3D printing was excellent shelf-stability of the TTA-UC resin, with no change in photopolymerization performance observed during a 45-day study.

Our work additionally poses several exciting fundamental questions and prospective avenues to examine and leverage TTA-UC in photopolymerizations. For example, we observed polymerization in the absence of BAPO initiator and speculated that it was driven by electron transfer from high-energy triplet pair states to 2-phenoxyethylacrylate monomers. As this represents a new pathway for upconversion-driven chemistry to operate

beyond the spin-statistics constraints of traditional $^1[\text{An}]^*$ formation,^{41,57} it could provide a new paradigm in photopolymerizations that do not require traditional initiators. Additionally, alternative **PS**, **An**, and **I** pairs can be examined to eliminate the use of precious metals,^{58,59} while increasing Φ_{UC} , r_p , and anti-stokes shift to reduce energetic losses, widen the range of excitation wavelengths, increase photocuring efficiency, and improve 3D printing speed and resolution. As a result, we anticipate TTA-UC to Type I photocuring can be harnessed to enable benign and wavelength-selective fabrication of multifunctional materials with potential applications in medicine, from tissue engineering for improved disease models and soft actuators for human-interfaced robotics and electronics.

AUTHOR INFORMATION

Corresponding Author

Zachariah A. Page – Department of Chemistry, The University of Texas at Austin, Austin, Texas 78712, USA.

Email: zpage@utexas.edu

Sean T. Roberts – Department of Chemistry, The University of Texas at Austin, Austin, Texas 78712, USA.

Email: roberts@cm.utexas.edu

Author Contributions

Conceptualization (**STR**, **ZAP**); Methodology (**CJO**, **JI**, **STR**, **ZAP**); Investigation (**CJO**, **JI**, **EEC**); Visualization (**CJO**, **JI**, **EEC**, **STR**, **ZAP**); Funding acquisition (**STR**, **ZAP**); Project administration (**ZAP**); Supervision (**STR**, **ZAP**); Writing – original draft (**CJO**, **JI**); Writing – review & editing (**CJO**, **JI**, **STR**, **ZAP**).

ACKNOWLEDGMENT

The authors acknowledge primary support from the National Science Foundation under Grant No. CAT-2155017 (**CJO**, **JI**, **EEC**, **STR**, **ZAP**). Partial support was provided by the Robert A. Welch Foundation under Grant No. F-2007 (**CJO**, **EEC**, **ZAP**) and F-1885 (**JI**, **STR**) and Research Corporation for Science Advancement under Award #28184 (**CJO**, **EEC**, **ZAP**).

ABBREVIATIONS

LED, light emitting diode; DLP, digital light processing; I_{scatter} , scattered light intensity; r_p , rate of polymerization; I_{ex} , excitation intensity; TTA, triplet-triplet annihilation; UC, upconversion; PS, photosensitizer; PtOEP, platinum octaethylporphyrin; DPA, diphenylanthracene; An, annihilator; TET, triplet energy transfer; I, initiator; BAPO, bisacylphosphine oxide; A, electron acceptor; D, electron donor; PhOEA, 2-phenoxyethylacrylate; ISC, intersystem crossing; Ox, oxidation; Red, reduction; M, monomer; P_n, polymer; Φ_{UC} , upconversion quantum efficiency; I_{th} , intensity threshold; k_{An}^{T} , $^3[\text{An}]^*$ decay rate constant; α , PS absorption coefficient; ϕ_{TET} , $^3[\text{PS}]^*$ to $^1[\text{An}]$ TET efficiency; γ_{TTA} , TTA second-order rate constant. ϕ_{ISC} , ISC efficiency of **PS**; ϕ_{TTA} , TTA quantum yield; f , spin-statistical factor; ϕ_{fl} , fluorescence quantum yield of **An**; BP, bandpass; RT, real-time; FTIR, Fourier transform infrared spectroscopy; ATR, attenuated total reflectance; ρ , monomer to polymer conversion; ρ_{max} , maximum conversion; η , viscosity; t_{inh} , inhibition time; t_{50} , time to reach 50% conversion; TMPTA, trimethylolpropane triacrylate; C_d , cure depth; E_c , critical exposure; D_p , depth of penetration; E_0 , total light energy; FWHM, full width at half maximum.

REFERENCES

- Corrigan, N.; Yeow, J.; Judzewitsch, P.; Xu, J.; Boyer, C. Seeing the Light: Advancing Materials Chemistry through Photopolymerization. *Angew. Chemie Int. Ed.* **2019**, *58* (16), 5170–5189. <https://doi.org/10.1002/anie.201805473>.
- Dadashi-Silab, S.; Doran, S.; Yagci, Y. Photoinduced Electron Transfer Reactions for Macromolecular Syntheses. *Chem. Rev.* **2016**, *116* (17), 10212–10275. <https://doi.org/10.1021/acs.chemrev.5b00586>.
- Bao, Y. Recent Trends in Advanced Photoinitiators for Vat Photopolymerization 3D Printing. *Macromol. Rapid Commun.* **2022**, *43* (14), 2200202. <https://doi.org/10.1002/marc.202200202>.
- Liddle, J. A.; Gallatin, G. M. Nanomanufacturing: A Perspective. *ACS Nano* **2016**, *10* (3), 2995–3014. <https://doi.org/10.1021/acsnano.5b03299>.
- Zhang, F.; Zhu, L.; Li, Z.; Wang, S.; Shi, J.; Tang, W.; Li, N.; Yang, J. The Recent Development of Vat Photopolymerization: A Review. *Addit. Manuf.* **2021**, *48*, 102423. <https://doi.org/10.1016/j.addma.2021.102423>.
- Xu, X.; Awad, A.; Robles-Martinez, P.; Gaisford, S.; Goyanes, A.; Basit, A. W. Vat Photopolymerization 3D Printing for Advanced Drug Delivery and Medical Device Applications. *J. Control. Release* **2021**, *329*, 743–757. <https://doi.org/10.1016/j.jconrel.2020.10.008>.
- Lu, P.; Ahn, D.; Yunis, R.; Delafresnaye, L.; Corrigan, N.; Boyer, C.; Barner-Kowollik, C.; Page, Z. A. Wavelength-Selective Light-Matter Interactions in Polymer Science. *Matter* **2021**, *4* (7), 2172–2229. <https://doi.org/10.1016/j.matt.2021.03.021>.
- Bagheri, A.; Jin, J. Photopolymerization in 3D Printing. *ACS Appl. Polym. Mater.* **2019**, *1* (4), 593–611. <https://doi.org/10.1021/acsapm.8b00165>.
- Li, J.; Boyer, C.; Zhang, X. 3D Printing Based on Photopolymerization and Photocatalysts: Review and Prospect.

- Macromol. Mater. Eng.* **2022**, *307* (8), 2200010. <https://doi.org/10.1002/mame.202200010>.
- (10) Müller, S. M.; Schlögl, S.; Wiesner, T.; Haas, M.; Griesser, T. Recent Advances in Type I Photoinitiators for Visible Light Induced Photopolymerization. *ChemPhotoChem* **2022**, *6* (11), e202200091. <https://doi.org/10.1002/cptc.202200091>.
 - (11) Stevens, L. M.; Recker, E. A.; Zhou, K. A.; Garcia, V. G.; Mason, K. S.; Tagnon, C.; Abdelaziz, N.; Page, Z. A. Counting All Photons: Efficient Optimization of Visible Light 3D Printing. *Adv. Mater. Technol.* **2023**, 2300052. <https://doi.org/10.1002/admt.202300052>.
 - (12) Stevens, L. M.; Tagnon, C.; Page, Z. A. “Invisible” Digital Light Processing 3D Printing with Near Infrared Light. *ACS Appl. Mater. Interfaces* **2022**, *14* (20), 22912–22920. <https://doi.org/10.1021/acscami.1c22046>.
 - (13) Ahn, D.; Stevens, L. M.; Zhou, K.; Page, Z. A. Additives for Ambient 3D Printing with Visible Light. *Adv. Mater.* **2021**, *33* (44), 2104906. <https://doi.org/10.1002/adma.202104906>.
 - (14) Ahn, D.; Stevens, L. M.; Zhou, K.; Page, Z. A. Rapid High-Resolution Visible Light 3D Printing. *ACS Cent. Sci.* **2020**, *6* (9), 1555–1563. <https://doi.org/10.1021/acscentsci.0c00929>.
 - (15) Stafford, A.; Ahn, D.; Raulerson, E. K.; Chung, K. Y.; Sun, K.; Cadena, D. M.; Forrister, E. M.; Yost, S. R.; Roberts, S. T.; Page, Z. A. Catalyst Halogenation Enables Rapid and Efficient Polymerizations with Visible to Far-Red Light. *J. Am. Chem. Soc.* **2020**. <https://doi.org/10.1021/jacs.0c07136>.
 - (16) Wu, C.; Corrigan, N.; Lim, C.-H.; Liu, W.; Miyake, G.; Boyer, C. Rational Design of Photocatalysts for Controlled Polymerization: Effect of Structures on Photocatalytic Activities. *Chem. Rev.* **2022**, *122* (6), 5476–5518. <https://doi.org/10.1021/acs.chemrev.1c00409>.
 - (17) O’Halloran, S.; Pandit, A.; Heise, A.; Kellett, A. Two-Photon Polymerization: Fundamentals, Materials, and Chemical Modification Strategies. *Adv. Sci.* **2023**, *10* (7), 2204072. <https://doi.org/10.1002/advs.202204072>.
 - (18) Hahn, V.; Bojanowski, N. M.; Rietz, P.; Feist, F.; Kozłowska, M.; Wenzel, W.; Blasco, E.; Bräse, S.; Barner-Kowollik, C.; Wegener, M. Challenges and Opportunities in 3D Laser Printing Based on (1 + 1)-Photon Absorption. *ACS Photonics* **2023**, *10* (1), 24–33. <https://doi.org/10.1021/acsp Photonics.2c01632>.
 - (19) Wei, L.; Yang, C.; Wu, W. Recent Advances of Stereolithographic 3D Printing Enabled by Photon Upconversion Technology. *Curr. Opin. Green Sustain. Chem.* **2023**, *43*, 100851. <https://doi.org/10.1016/j.cogsc.2023.100851>.
 - (20) Schloemer, T.; Narayanan, P.; Zhou, Q.; Belliveau, E.; Seitz, M.; Congreve, D. N. Nanoengineering Triplet–Triplet Annihilation Upconversion: From Materials to Real-World Applications. *ACS Nano* **2023**, *17* (4), 3259–3288. <https://doi.org/10.1021/acsnano.3c00543>.
 - (21) Hahn, V.; Kiefer, P.; Frenzel, T.; Qu, J.; Blasco, E.; Barner-Kowollik, C.; Wegener, M. Rapid Assembly of Small Materials Building Blocks (Voxels) into Large Functional 3D Metamaterials. *Adv. Funct. Mater.* **2020**, *30* (26), 1907795. <https://doi.org/10.1002/adfm.201907795>.
 - (22) Zhao, Z.; Tian, X.; Song, X. Engineering Materials with Light: Recent Progress in Digital Light Processing Based 3D Printing. *J. Mater. Chem. C* **2020**, *8* (40), 13896–13917. <https://doi.org/10.1039/D0TC03548C>.
 - (23) Feng, J.; Alves, J.; de Clercq, D. M.; Schmidt, T. W. Photochemical Upconversion. *Annu. Rev. Phys. Chem.* **2023**, *74* (1), 145–168. <https://doi.org/10.1146/annurev-physchem-092722-104952>.
 - (24) Ravetz, B. D.; Pun, A. B.; Churchill, E. M.; Congreve, D. N.; Rovis, T.; Campos, L. M. Photoredox Catalysis Using Infrared Light via Triplet Fusion Upconversion. *Nature* **2019**, *565* (7739), 343–346. <https://doi.org/10.1038/s41586-018-0835-2>.
 - (25) Awwad, N.; Bui, A. T.; Danilov, E. O.; Castellano, F. N. Visible-Light-Initiated Free-Radical Polymerization by Homomolecular Triplet–Triplet Annihilation. *Chem* **2020**, *6* (11), 3071–3085. <https://doi.org/10.1016/j.chempr.2020.08.019>.
 - (26) Caron, A.; Noirbent, G.; Gimes, D.; Dumur, F.; Lalevée, J. Near-Infrared PhotoInitiating Systems: Photothermal versus Triplet–Triplet Annihilation-Based Upconversion Polymerization. *Macromol. Rapid Commun.* **2021**, *42* (11), 2100047. <https://doi.org/10.1002/marc.202100047>.
 - (27) Wang, Z.; Hou, Y.; Huo, Z.; Liu, Q.; Xu, W.; Zhao, J. Spatially Confined Photoexcitation with Triplet–Triplet Annihilation Upconversion. *Chem. Commun.* **2021**, *57* (72), 9044–9047. <https://doi.org/10.1039/D1CC03309C>.
 - (28) Fu, Q.; Rui, J.; Fang, J.; Ni, Y.; Fang, L.; Lu, C.; Xu, Z. Triplet–Triplet Annihilation Up-Conversion Luminescent Assisted Free-Radical Reactions of Polymers Using Visible Light. *Macromol. Chem. Phys.* **2022**, *223* (14), 2200038. <https://doi.org/10.1002/macp.202200038>.
 - (29) Liang, W.; Nie, C.; Du, J.; Han, Y.; Zhao, G.; Yang, F.; Liang, G.; Wu, K. Near-Infrared Photon Upconversion and Solar Synthesis Using Lead-Free Nanocrystals. *Nat. Photonics* **2023**, *17* (4), 346–353. <https://doi.org/10.1038/s41566-023-01156-6>.
 - (30) Wong, J.; Wei, S.; Meir, R.; Sadaba, N.; Ballinger, N. A.; Harmon, E. K.; Gao, X.; Altin-Yavuzarslan, G.; Pozzo, L. D.; Campos, L. M.; Nelson, A. Triplet Fusion Upconversion for Photocuring 3D-Printed Particle-Reinforced Composite Networks. *Adv. Mater.* **2023**, *35* (11), 2207673. <https://doi.org/10.1002/adma.202207673>.
 - (31) Wei, Y.; Pan, K.; Cao, X.; Li, Y.; Zhou, X.; Yang, C. Multiple Resonance Thermally Activated Delayed Fluorescence Sensitizers Enable Green-to-Ultraviolet Photon Upconversion: Application in Photochemical Transformations. *CCS*

- Chem.* **2022**, *4* (12), 3852–3863. <https://doi.org/10.31635/ccschem.022.202101507>.
- (32) Sanders, S. N.; Schloemer, T. H.; Gangishetty, M. K.; Anderson, D.; Seitz, M.; Gallegos, A. O.; Stokes, R. C.; Congreve, D. N. Triplet Fusion Upconversion Nanocapsules for Volumetric 3D Printing. *Nature* **2022**, *604* (7906), 474–478. <https://doi.org/10.1038/s41586-022-04485-8>.
- (33) Limberg, D. K.; Kang, J.-H.; Hayward, R. C. Triplet–Triplet Annihilation Photopolymerization for High-Resolution 3D Printing. *J. Am. Chem. Soc.* **2022**, *144* (12), 5226–5232. <https://doi.org/10.1021/jacs.1c11022>.
- (34) Wang, Z.; Zhang, Y.; Su, Y.; Zhang, C.; Wang, C. Three-Dimensional Direct-Writing via Photopolymerization Based on Triplet–Triplet Annihilation. *Sci. China Chem.* **2022**, *65* (11), 2283–2289. <https://doi.org/10.1007/s11426-022-1380-6>.
- (35) Luo, Z.; Wang, D.; Li, K.; Zhong, D.; Xue, L.; Gan, Z.; Xie, C. Three-Dimensional Nanolithography with Visible Continuous Wave Laser through Triplet Up-Conversion. *J. Phys. Chem. Lett.* **2023**, *14* (3), 709–715. <https://doi.org/10.1021/acs.jpcclett.2c03601>.
- (36) Brinen, J. S.; Koren, J. G. The Lowest Triplet State of 9, 10 Diphenylanthracene. *Chem. Phys. Lett.* **1968**, *2* (8), 671–672. [https://doi.org/10.1016/0009-2614\(63\)80050-0](https://doi.org/10.1016/0009-2614(63)80050-0).
- (37) Fiege, H.; Voges, H.; Hamamoto, T.; Umemura, S.; Iwata, T.; Miki, H.; Fujita, Y.; Buysch, H.; Garbe, D.; Paulus, W. Phenol Derivatives. In *Ullmann's Encyclopedia of Industrial Chemistry*; Wiley, 2000. https://doi.org/10.1002/14356007.a19_313.
- (38) Monguzzi, A.; Tubino, R.; Hoseinkhani, S.; Campione, M.; Meinardi, F. Low Power, Non-Coherent Sensitized Photon up-Conversion: Modelling and Perspectives. *Phys. Chem. Chem. Phys.* **2012**, *14* (13), 4322. <https://doi.org/10.1039/c2cp23900k>.
- (39) Cheng, Y. Y.; Fückel, B.; Khoury, T.; Clady, R. G. C. R.; Tayebjee, M. J. Y.; Ekins-Daukes, N. J.; Crossley, M. J.; Schmidt, T. W. Kinetic Analysis of Photochemical Upconversion by Triplet–Triplet Annihilation: Beyond Any Spin Statistical Limit. *J. Phys. Chem. Lett.* **2010**, *1* (12), 1795–1799. <https://doi.org/10.1021/jz100566u>.
- (40) Bossanyi, D. G.; Matthiesen, M.; Wang, S.; Smith, J. A.; Kilbride, R. C.; Shipp, J. D.; Chekulaev, D.; Holland, E.; Anthony, J. E.; Zaumseil, J.; Musser, A. J.; Clark, J. Emissive Spin-0 Triplet-Pairs Are a Direct Product of Triplet–Triplet Annihilation in Pentacene Single Crystals and Anthradithiophene Films. *Nat. Chem.* **2021**, *13* (2), 163–171. <https://doi.org/10.1038/s41557-020-00593-y>.
- (41) Bossanyi, D. G.; Sasaki, Y.; Wang, S.; Chekulaev, D.; Kimizuka, N.; Yanai, N.; Clark, J. Spin Statistics for Triplet–Triplet Annihilation Upconversion: Exchange Coupling, Intermolecular Orientation, and Reverse Intersystem Crossing. *JACS Au* **2021**, *1* (12), 2188–2201. <https://doi.org/10.1021/jacsau.1c00322>.
- (42) Monguzzi, A.; Mezyk, J.; Scotognella, F.; Tubino, R.; Meinardi, F. Upconversion-Induced Fluorescence in Multicomponent Systems: Steady-State Excitation Power Threshold. *Phys. Rev. B* **2008**, *78* (19), 195112. <https://doi.org/10.1103/PhysRevB.78.195112>.
- (43) Chattopadhyay, S. K.; Kumar, C. V.; Das, P. K. Triplet-Related Photophysics of 9,10-Diphenylanthracene. A Kinetic Study of Reversible Energy Transfer from Anthracene Triplet by Nanosecond Laser Flashes. *Chem. Phys. Lett.* **1983**, *98* (3), 250–254. [https://doi.org/10.1016/0009-2614\(83\)87160-7](https://doi.org/10.1016/0009-2614(83)87160-7).
- (44) Bharmoria, P.; Bildirir, H.; Moth-Poulsen, K. Triplet–Triplet Annihilation Based near Infrared to Visible Molecular Photon Upconversion. *Chem. Soc. Rev.* **2020**, *49* (18), 6529–6554. <https://doi.org/10.1039/D0CS00257G>.
- (45) Edhborg, F.; Olesund, A.; Albinsson, B. Best Practice in Determining Key Photophysical Parameters in Triplet–Triplet Annihilation Photon Upconversion. *Photochem. Photobiol. Sci.* **2022**, *21* (7), 1143–1158. <https://doi.org/10.1007/s43630-022-00219-x>.
- (46) Olesund, A.; Gray, V.; Mårtensson, J.; Albinsson, B. Diphenylanthracene Dimers for Triplet–Triplet Annihilation Photon Upconversion: Mechanistic Insights for Intramolecular Pathways and the Importance of Molecular Geometry. *J. Am. Chem. Soc.* **2021**, *143* (15), 5745–5754. <https://doi.org/10.1021/jacs.1c00331>.
- (47) Yanai, N.; Suzuki, K.; Ogawa, T.; Sasaki, Y.; Harada, N.; Kimizuka, N. Absolute Method to Certify Quantum Yields of Photon Upconversion via Triplet–Triplet Annihilation. *J. Phys. Chem. A* **2019**, *123* (46), 10197–10203. <https://doi.org/10.1021/acs.jpca.9b08636>.
- (48) Carmona, P.; Moreno, J. The Infrared Spectra and Structure of Methyl Acrylate. *J. Mol. Struct.* **1982**, *82* (3–4), 177–185. [https://doi.org/10.1016/0022-2860\(82\)80033-1](https://doi.org/10.1016/0022-2860(82)80033-1).
- (49) Kim, J.-H.; Deng, F.; Castellano, F. N.; Kim, J.-H. High Efficiency Low-Power Upconverting Soft Materials. *Chem. Mater.* **2012**, *24* (12), 2250–2252. <https://doi.org/10.1021/cm3012414>.
- (50) Leatherdale, C. A.; DeVoe, R. J. Two-Photon Microfabrication Using Two-Component Photoinitiation Systems: Effect of Photosensitizer and Acceptor Concentrations. *Nonlinear Opt. Transm. Multiphot. Process. Org.* **2003**, *5211*, 112–123. <https://doi.org/10.1117/12.508087>.
- (51) Tryson, G. R.; Shultz, A. R. A Calorimetric Study of Acrylate Photopolymerization. *J. Polym. Sci. Polym. Phys. Ed.* **1979**, *17* (12), 2059–2075. <https://doi.org/10.1002/pol.1979.180171202>.
- (52) Lovelh, L. G.; Newman, S. M.; Bowman, C. N. The Effects of Light Intensity, Temperature, and Comonomer Composition on the Polymerization Behavior of Dimethacrylate Dental Resins. *J. Dent. Res.* **1999**, *78* (8), 1469–1476.

- <https://doi.org/10.1177/00220345990780081301>.
- (53) Rau, D. A.; Reynolds, J. P.; Bryant, J. S.; Bortner, M. J.; Williams, C. B. A Rheological Approach for Measuring Cure Depth of Filled and Unfilled Photopolymers at Additive Manufacturing Relevant Length Scales. *Addit. Manuf.* **2022**, *60*, 103207. <https://doi.org/10.1016/j.addma.2022.103207>.
- (54) Jacobs, P. F. Rapid Prototyping & Manufacturing— Fundamentals of Stereolithography. *J. Manuf. Syst.* **1993**, *12* (5), 430–433. [https://doi.org/10.1016/0278-6125\(93\)90311-g](https://doi.org/10.1016/0278-6125(93)90311-g).
- (55) Bennett, J. Measuring UV Curing Parameters of Commercial Photopolymers Used in Additive Manufacturing. *Addit. Manuf.* **2017**, *18*, 203–212. <https://doi.org/10.1016/j.addma.2017.10.009>.
- (56) Champion, A.; Metral, B.; Schuller, A.; Croutxé-Barghorn, C.; Ley, C.; Halbardier, L.; Allonas, X. A Simple and Efficient Model to Determine the Photonic Parameters of a Photopolymerizable Resin Usable in 3D Printing. *ChemPhotoChem* **2021**, *5* (9), 839–846. <https://doi.org/10.1002/cptc.202100002>.
- (57) Schulze, T. F.; Schmidt, T. W. Photochemical Upconversion: Present Status and Prospects for Its Application to Solar Energy Conversion. *Energy Environ. Sci.* **2015**, *8* (1), 103–125. <https://doi.org/10.1039/c4ee02481h>.
- (58) Uji, M.; Harada, N.; Kimizuka, N.; Saigo, M.; Miyata, K.; Onda, K.; Yanai, N. Heavy Metal-Free Visible-to-UV Photon Upconversion with over 20% Efficiency Sensitized by a Ketocoumarin Derivative. *J. Mater. Chem. C* **2022**, *10* (12), 4558–4562. <https://doi.org/10.1039/D1TC05526G>.
- (59) Chen, Z.; Mahmood, Z.; Liang, H.; Wen, Y.; Huo, Y.; Ji, S. Efficient Red Light Polymerization Facilitated by Low Energy Excitation Based on a Single-Atom Substituted Naphthalimide. *Dye. Pigment.* **2023**, *219*, 111636. <https://doi.org/10.1016/j.dyepig.2023.111636>.